PHOTONICS Research

Multigigawatt 50 fs Yb:CALGO regenerative amplifier system with 11 W average power and mid-infrared generation

Weizhe Wang,[1] Han Wu,[1] Cheng Liu,[2] Biao Sun,[3] and Houkun Liang[1,*]

[1]College of Electronics and Information Engineering, Sichuan University, Chengdu 610064, China
[2]Beijing WaveQuanta Technology Co., Ltd., Beijing 102208, China
[3]Hangzhou Yacto Technology Ltd., Hangzhou 311305, China
*Corresponding author: hkliang@scu.edu.cn

Received 18 March 2021; revised 28 May 2021; accepted 31 May 2021; posted 1 June 2021 (Doc. ID 425149); published 8 July 2021

Lasers with high average and high peak power as well as ultrashort pulse width have been all along demanded by nonlinear optics studies, strong-field experiments, electron dynamics investigations, and ultrafast spectroscopy. While the routinely used titanium-doped sapphire (Ti:sapphire) laser faces a bottleneck in the average power upscaling, ytterbium (Yb)-doped lasers have remarkable advantages in achieving high average power. However, there is still a substantial gap of pulse width and peak power between the Ti:sapphire and Yb-doped lasers. Here we demonstrate a high-power Yb:$CaAlGdO_4$ (Yb:CALGO) regenerative amplifier system, delivering 1040 nm pulses with 11 W average power, 50 fs pulse width, and 3.7 GW peak power at a repetition rate of 43 kHz, which to some extent bridges the gap between the Ti:sapphire and Yb lasers. An ultrabroadband Yb-doped fiber oscillator, specially designed spectral shapers, and Yb:CALGO gain medium with broad emission bandwidth, together with a double-end pumping scheme enable an amplified bandwidth of 19 nm and 95 fs output pulse width. To the best of our knowledge, this is the first demonstration of sub-100 fs regenerative amplifier based on Yb-doped bulk medium without nonlinear spectral broadening. The amplified pulse is further compressed to 50 fs via cascaded-quadratic compression with a simple setup, producing 3.7 GW peak power, which boosts the record of peak power from Yb:CALGO regenerative amplifiers by 1 order. As a proof of concept, pumped by the high-power, 50 fs pulses, 7.5–11.5 μm mid-infrared (MIR) generation via intrapulse difference-frequency generation is performed, without the necessity of nonlinear fiber compressors. It leads to a simple and robust apparatus, and it would find good usefulness in MIR spectroscopic applications.

https://doi.org/10.1364/PRJ.425149

1. INTRODUCTION

High-peak-power and average-power lasers with ultrashort pulse width are the enablers for a number of important applications such as wavelength conversions into deep ultraviolet [1], mid-infrared (MIR) [2,3], and terahertz bands [4]; strong-field experiments including high-harmonic generation [5], attosecond pulse generation [6]; and two-dimensional spectroscopy [7]. While titanium-doped sapphire (Ti:sapphire) lasers with high peak power and sub-50 fs pulse width have been routinely employed as the unanimous driving sources, upscaling the average power to the scale > 10 W is technically challenging. However, for some typical applications, such as high-harmonic generation, attosecond pulse generation, and intrapulse difference-frequency generation (IPDFG), driven by Ti:sapphire lasers, a good average power is highly demanded for the required photon flux. Thus it is heavily desired to have a new driving laser source with hundreds of microjoules (μJ) or millijoule (mJ)-level pulse energy, > 10 W or multi-10 W average power, and sub-50 fs pulse width. On the other hand, in the last decade, ytterbium (Yb)-doped lasers have attained dramatic progress for a number of advantages. First, much smaller quantum defects pumped at ∼980 nm lead to significantly less heat accumulation. Second, Yb gain media could be pumped by widely available and less expensive high-power laser diodes. Moreover, the smaller thermal-optic coefficient ($\sim 8 \times 10^{-6}$ K^{-1} [8] for Yb versus $\sim 13 \times 10^{-6}$ K^{-1} [9] for Ti:sapphire) means the reduced thermal sensitivity at a high power operation. Thus, ∼1 ps pulses with joule-level pulse energy and kilowatt (kW) average power have been generated in Yb:YAG lasers with thin disk [10], cryogenic-cooling [11], or InnoSlab [12] techniques. However, there is still a substantial gap of pulse width and peak power between the Ti:sapphire and Yb-doped lasers.

To bridge the gap, a number of Yb gain media such as Yb:CaF_2 (emission bandwidth $\Delta\lambda_e \sim 70$ nm) [13,14],

Yb:KGW ($\Delta\lambda_e \sim 20$–25 nm) [15–17], Yb:$CaAlGdO_4$ (Yb:CALGO) ($\Delta\lambda_e \sim 80$ nm) [18–20], Yb:CALYO ($\Delta\lambda_e \sim 80$ nm) [21,22], and Yb:Lu_2O_3 ($\Delta\lambda_e \sim 12$ nm) [23,24] with broad emission bandwidth have been explored. Among all the aforementioned Yb gain media, the thermal conductivity of Yb:CALGO [6.3 W/(m·K)] [25] is only lower than that of Yb:Lu_2O_3 [12 W/(m·K)] [23], whereas Yb:CALGO has a much broader emission bandwidth. Thus Yb:CALGO emerges as a promising candidate for the sub-100 fs or even sub-50 fs pulse generation with high peak power and average power. Kerr-lens mode-locked Yb:CALGO oscillators with sub-100 fs pulse width and < 3 MW peak power at a repetition rate of 40–80 MHz have been demonstrated [18,19]. To achieve higher pulse energy and peak power, the regenerative amplifier is adapted. An Yb:CALGO regenerative amplifier with 27 W average power, 54 μJ pulse energy, and 140 fs pulses at a repetition rate of 500 kHz has been demonstrated with 330 MW peak power [20]. With the aid of nonlinear spectral broadening in the Yb:CALGO regenerative amplifier cavity, a pulse duration down to 97 fs is obtained with an output power of 1.2 W at 50 kHz repetition rate, corresponding to a peak power of 218 MW [26]. However, sub-50 fs pulses with multigigawatt peak power, which are demanded by applications like strong-field experiments and parametric downconversions have not yet been realized.

One typical application of the sub-50 fs near-infrared driving source with high peak power is the MIR pulse generation via IPDFG. Driving lasers with the pulse width < 30 fs have been routinely used in MIR IPDFG [2,27–30]. Nonlinear fiber compressors accompanied with chirped mirrors [31] or multipass compressors [32] are thus required for the additional nonlinear compression with a high compression factor, but to some extent make the setup complex and increase the cost of the whole system too.

In this paper, we report a high-power Yb:CALGO regenerative amplification system, delivering 50 fs pulses centered at 1040 nm with 11 W average power and 3.7 GW peak power at a repetition rate of 43 kHz. Combining the ultrabroadband Yb-fiber oscillator, seed spectral shaper, double-end pumping scheme, and Yb:CALGO gain media, 95 fs pulses with 12.5 W average power are output directly from the regenerative amplifier. To the best of our knowledge, this is the first demonstration of sub-100 fs regenerative amplifier based on Yb-doped bulk medium, without nonlinear spectral broadening. In the normal dispersive regime, cascaded-quadratic compression has been a simple and cost effective technique that averts the necessity of expensive chirp mirrors and fine alignment [33,34]. The 95 fs output pulse is further compressed to 50 fs via cascaded-quadratic compression, with 11 W average power and 3.7 GW peak power. Subsequently, MIR emission tuning from 7.5 to 11.5 μm is generated through IPDFG in a long $LiGaS_2$ (LGS) crystal, which provides sufficient spectral broadening, serving as the signal of IPDFG. This is a proof-of-concept demonstration of MIR IPDFG driven by relatively long pulses without the necessity of nonlinear fiber compressors. It not only to a large extent simplifies the apparatus but also enhances the power efficiency, which could find good usefulness in MIR spectroscopic applications.

2. EXPERIMENTAL SETUP

As shown in Fig. 1, the experimental setup consists of four blocks, namely, front end, regenerative amplifier, cascaded-quadratic compressor, and MIR IPDFG stage, with the details presented as follows.

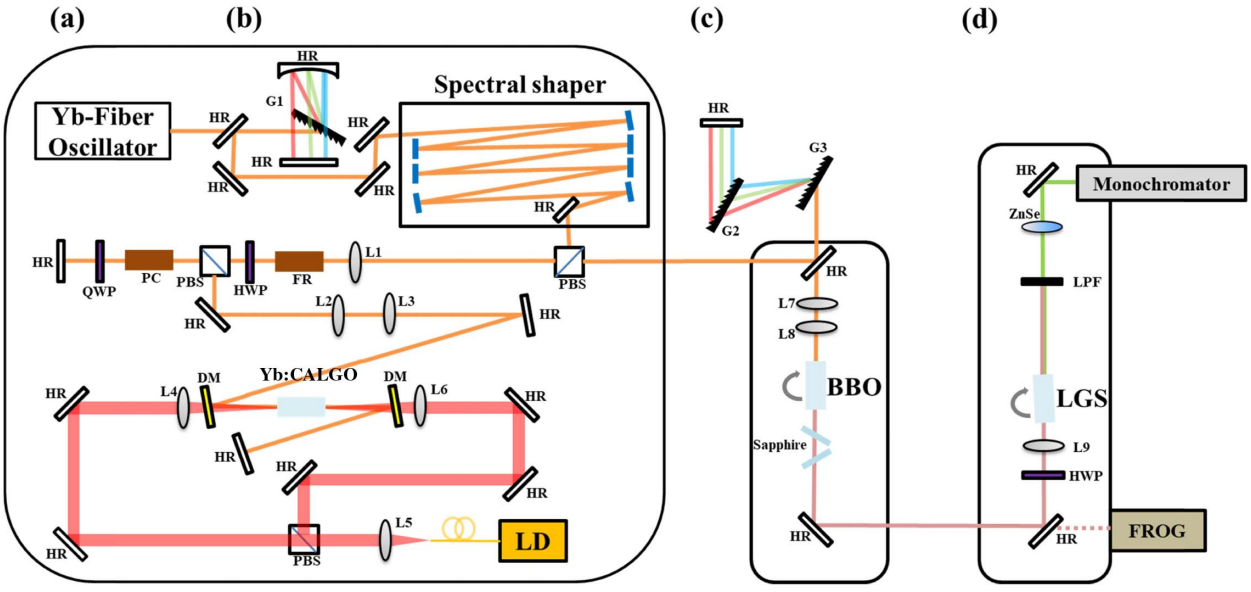

Fig. 1. Schematics of (a) front end, (b) regenerative amplifier, (c) cascaded-quadratic compressor, and (d) mid-infrared (MIR) intrapulse difference-frequency generation (IPDFG) stage. The front end consists of an Yb-fiber oscillator and a designed spectral shaper. The regenerative amplifier employs an Yb:CALGO crystal. HR, high reflection mirror; PBS, polarization beam splitter; L, lens; FR, Faraday rotator; HWP, half-wave plate; PC, Pockels cell; QWP, quarter-wave plate; DM, dichroic mirror; LD, laser diode; LPF, low-pass filter; G, high-efficiency transmission grating with 1600 lines/mm; LGS, $LiGaS_2$ crystal.

A. Front End

In the front end, a customized broadband Yb-fiber oscillator (Yacto-FL-Ultra) with the center wavelength of 1040 nm and −10 dB bandwidth of ∼70 nm is built to provide a seed pulse with broadband spectrum. Seed pulse trains with 1 nJ pulse energy are counted down to a repetition rate of 43 kHz with a high-contrast acoustic optical modulator. A Martinez stretcher with a group delay dispersion (GDD) of 3.5×10^6 fs^2 is employed to stretch the seed pulses to a width of ∼140 ps with an overall efficiency of ∼80%. To compensate for the strong gain narrowing in the regenerative amplifier, a notched spectral shaper is specially designed and employed after the stretcher to preshape the seed spectrum. The reflectivity of a single dielectric spectral shaper has a dip of 20% centered at 1040 nm, spanning in the spectral range of 1025–1055 nm. Seven-bounces reflection is designed in the seed spectral shaper. Finally, 80% of attenuation is achieved in the spectral center as depicted by the blue dotted curve in Fig. 2(a). A ∼0.2 nJ seed pulse is thus transmitted through the spectral shaper and injected into the regenerative cavity.

B. Regenerative Amplifier

A 1.5%-doped Yb:CALGO crystal with *a*-cut orientation and 8 mm thickness is mounted on a water-cooled copper holder with four surrounding cooling surfaces. Double-end pumping is adopted by using a fiber-coupled (core diameter of 200 μm) laser diode with a maximum output power of 240 W and the wavelength locked at 980 nm. In the cavity of the regenerative amplifier, which is 2 m in length, telescopes are used to precisely adjust the beam sizes at different optics and to ensure a stable operation. The beam diameters of pump and signal on the Yb:CALGO crystal are designed as ∼400 μm and ∼380 μm, respectively, to ensure a good gain performance and mitigate the risk of damage. The beam diameter is enlarged to ∼600 μm on the Pockels cell with double beta-barium borate (BBO) crystals (overall length of 40 mm) to avoid any nonlinear modulation. After amplification, the amplified pulse is then sent to a Treacy compressor providing a GDD of -4.5×10^6 fs^2 with an overall efficiency of 80%. The difference in GDD between the stretcher and compressor is mainly attributed to the accumulated dispersion of the Yb:CALGO crystal (0.7×10^6 fs^2) and 40 mm thick BBO (0.3×10^6 fs^2) in the Pockels cell, after 90 round trips. The amplified laser is characterized by an optical spectral analyzer (Yokogawa AQ6370D), a power meter (Ophir FL250A-BB-50), and a beam profiler (Dataray WinCamD).

C. Cascaded-Quadratic Compression

To further compress the amplified pulse, an antireflection (AR)-coated BBO crystal with the type I phase-matching angle of 23.5° and 20 mm thickness is used for the cascaded-quadratic compression. The beam size of the output pulse from the Treacy compressor is expanded to 2.6 mm on the BBO with another telescope, generating a peak intensity of ∼115 GW/cm^2. Two 9 mm thick sapphire crystals placed at the Brewster angle are carefully chosen to compensate for the negative GDD from the cascaded-quadratic compression process. The overall efficiency of the cascade nonlinear compression is 88%. The temporal profiles of the compressed pulses are characterized by a commercial second-harmonic generation frequency-resolved optical gating (SHG-FROG) setup (Mesa Photonics).

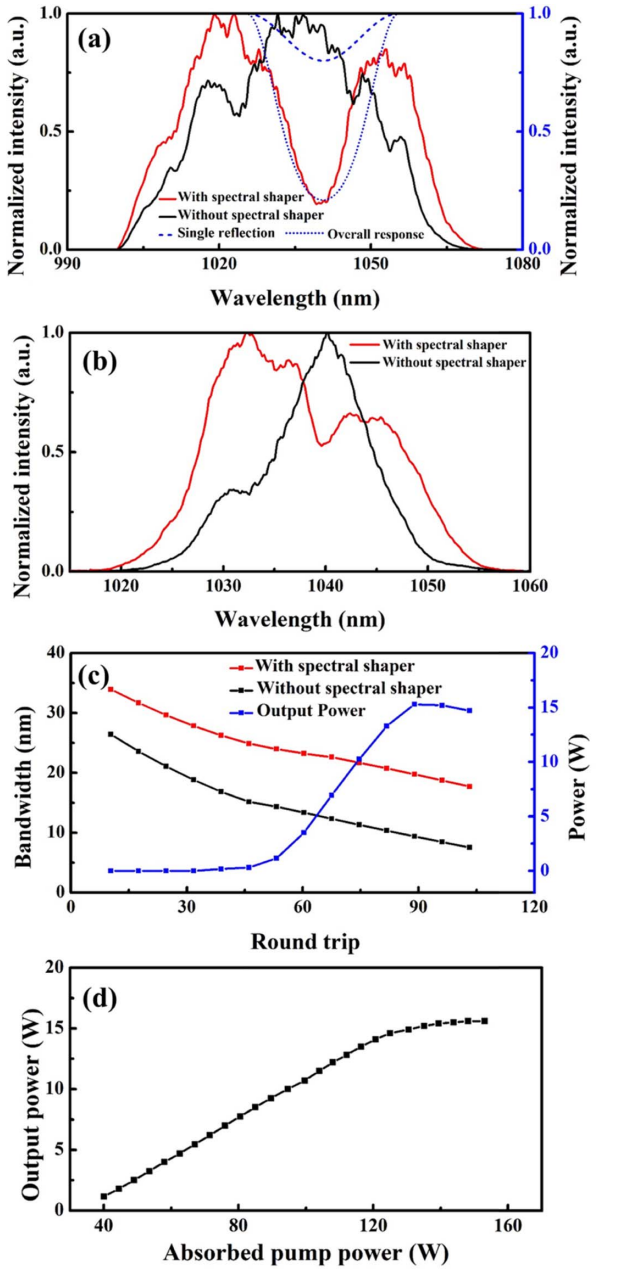

Fig. 2. (a) Comparison of the seed spectrum with (red) and without (black) the spectral shaper. The single reflection (blush dash) and overall response (blue dot) of the spectral shaper as a function of the wavelength are also included. (b) Comparison of the amplified spectrum with (red) and without (black) spectral shaping. The spectra correspond to the output power of ∼15.5 W with 90 round trips. (c) The amplified spectral bandwidth with (red) and without (black) the spectral shaper, and the output power (blue) as a function of the round trips in the regenerative amplifier, with the absorbed pump power of 150 W. (d) The amplified output power in the regenerative amplifier as a function of the absorbed pump power with 90 round trips.

D. MIR IPDFG

With the high-power ultrashort driving pulses, MIR downconversion via IPDFG is also investigated. An AR-coated 8 mm thick LGS crystal with the transparency range covering 0.32–11.6 μm and a bandgap energy of ~3.7 eV, which suppresses the two-photon absorption when pumped by the strong near-infrared pulses, is used. The type I phase-matching angle of 51° in the x–z plane is chosen for a broad phase-matching bandwidth, pumped at ~1040 nm wavelength, and small temporal walk-off between the pump and signal wavelengths. A half-wave plate (HWP) is employed to divide the pump beam into two orthogonally polarized components serving as the pump and signal beams. The beam diameter on the LGS crystal is 1.6 mm, corresponding to a peak intensity of ~230 GW/cm^2, which is below the measured damage threshold of 350 GW/cm^2 and 1000 GW/cm^2 reported in Ref. [27] and [2], respectively. It is to be noted that the power of the 50 fs driving laser used for the MIR IPDFG is limited to 5 W, to avoid any damage of the LGS crystal. The generated MIR pulses are separated from the residual near-infrared pump and signal using a long-pass filter with the cutoff wavelength at 3.6 μm. The long-wavelength MIR spectrum is then measured by using a scanning-grating monochromator with a liquid-nitrogen-cooled mercury cadmium telluride detector.

3. EXPERIMENT RESULTS AND DISCUSSION

A. Sub-100 fs Pulses from Yb Regenerative Amplifier

The seed spectra before and after the spectral shaper are characterized as presented in Fig. 2(a). The seed spectrum from the customized broadband Yb-fiber oscillator spans from 1000 to 1070 nm, which matches well with the emission bandwidth of the Yb:CALGO gain media. With seven bounces from the spectral shaper, the seed spectrum is shaped, forming a spectral hole with ~20% residual intensity centered at 1040 nm. The gain narrowing during amplification in the regenerative amplifier is significantly suppressed with the implementation of the spectral shaper and double-end pumping scheme, which increases the averaged inversion along the thick Yb:CALGO crystal [35] as compared in Fig. 2(b). The bandwidth of the amplified spectrum is increased from 9 to 19 nm with the aid of the spectral shaper, when 150 W pump power is absorbed. The spectral narrowing with respect to the amplification round trips is also characterized as presented in Fig. 2(c). It is observed that the amplified bandwidth is doubled with the spectral shaper at large round trips (> 60), indicating its crucial role in achieving the broad lasing bandwidth at high-gain operation. It is worth mentioning that the spectral shaper has negligible effect on the output power thanks to the high gain of the regenerative amplifier. With an absorbed pump power of 150 W and 90 round trips, the output power is saturated at 15.5 W at 43 kHz repetition rate, corresponding to 360 μJ pulse energy as shown in Figs. 2(c) and 2(d). A perfect Gaussian beam is manifested as shown in Fig. 3(a), indicating good thermal management of the regenerative amplifier.

The amplified pulses from the regenerative amplifier are compressed by a Treacy grating compressor with ~80% efficiency, generating 12.5 W, 290 μJ output pulses. The temporal

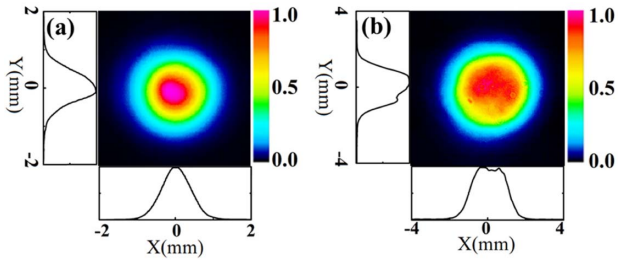

Fig. 3. Measured output beam profiles from (a) the Yb:CALGO regenerative amplifier and (b) the cascaded-quadratic compressor.

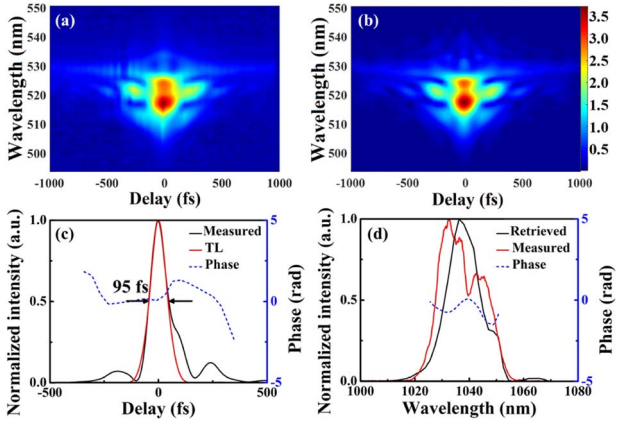

Fig. 4. SHG-FROG measurement of the 95 fs pulses from the regenerative amplifier. The (a) measured and (b) retrieved FROG traces of the 95 fs pulse. The FROG error is 0.8%. (c) The retrieved temporal profile and the transform-limited temporal profile. (d) The retrieved FROG spectral intensity and phase of the 95 fs laser pulse, compared to the spectrum independently measured using a spectral analyzer.

profile of the output pulse characterized by SHG-FROG is shown in Fig. 4. The measured and retrieved spectra have a relatively good agreement as presented in Fig. 4(d), with a bandwidth of 19 nm which supports a transform-limited (TL) pulse of 86 fs, assuming a Gaussian profile. The retrieved temporal profile shows a pulse width of 95 fs as presented in Fig. 4(c). The unsuppressed pedestals, which hold ~14% of the total energy from the measured pulse, account for the uncompensated third-order dispersion originated from the regenerative amplifier cavity. It is worth mentioning that this is the first demonstration of sub-100 fs output from an Yb-bulk regenerative amplifier without nonlinear modulation, to the best of our knowledge.

B. 50 fs Pulses from Cascaded-Quadratic Compression

More advanced applications such as MIR pulse generation via IPDFG require even shorter pulses from high-power regenerative amplifiers. With the cascaded-quadratic compression technique, a long BBO crystal with 20 mm thickness is employed to provide the required phase mismatch in an SHG conversion. The 12.5 W, 290 μJ, 95 fs pulses are incident on the BBO crystal with a peak intensity of ~115 GW/cm^2, which is

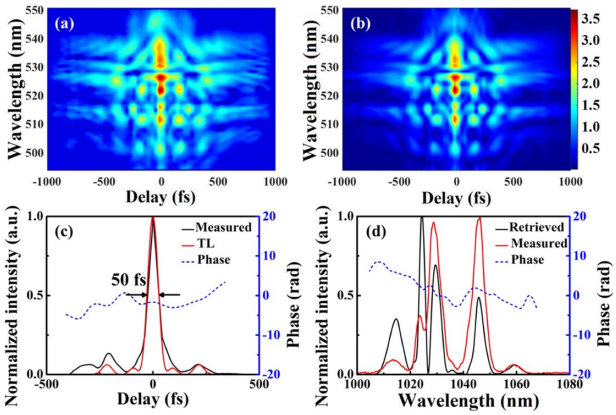

Fig. 5. SHG-FROG measurement of the 50 fs pulses from the cascaded-quadratic compressor. The (a) measured and (b) retrieved FROG traces of the 50 fs pulse. The FROG error is 0.95%. (c) The retrieved temporal profile and the transform-limited temporal profile. (d) The retrieved FROG spectral intensity and phase of the 50 fs laser pulse, compared to the spectrum independently measured using a spectral analyzer.

designed to generate a negative nonlinear phase shift for a two-fold pulse compression. It is worth mentioning that higher compression ratio is attainable, but incurable strong pedestals may emerge, which are caused by the uncompensated higher-order dispersion and could hold more than 30% of the total pulse energy. The GDD raised in the cascaded-quadratic compression process is calculated as -1500 fs^2. With 840 fs^2 GDD accumulated in the 20 mm thick BBO, two 9 mm thick sapphire crystals placed at the Brewster angle are carefully chosen to compensate the excess GDD. The temporal profile of the pulse after the cascaded-quadratic compressor is characterized by SHG-FROG as shown in Fig. 5. The spectrum is significantly broadened with modulations as presented in Fig. 5(d), which supports a TL pulse width of 48 fs, assuming a Gaussian temporal profile. As shown in Fig. 5(c), a 50 fs pulse width is measured with some weak pedestals emerging, which agrees well with our design. The pedestals contain ~23% of the total energy, which are caused by the nonuniform phase of the modulated spectrum. As a result, 11 W, 255 μJ, 50 fs pulses are obtained from the cascaded-quadratic compressor with an efficiency of 88%, which enhances the output peak power from 2.45 to 3.7 GW. The beam profile is also characterized as shown in Fig. 3(b). A uniform beam with a super-Gaussian shape is measured, which is attributed to the self-defocusing nonlinearity in the cascaded-quadratic compressor. It also indicates that there is no obvious spatial chirp generated in the compression process.

C. MIR Generation in LGS Crystal

For MIR generation via IPDFG, short pulses with a duration of 10–30 fs, compressed by a noble gas filled hollow-core fiber or photonic crystal fiber together with chirp mirrors, have been routinely used as the driving sources. To explore a simpler technique without the necessity of fiber compressors, MIR IPDFG driven by the 50 fs pulses is investigated for the first time to the best of our knowledge. The LGS crystal is chosen for its broad

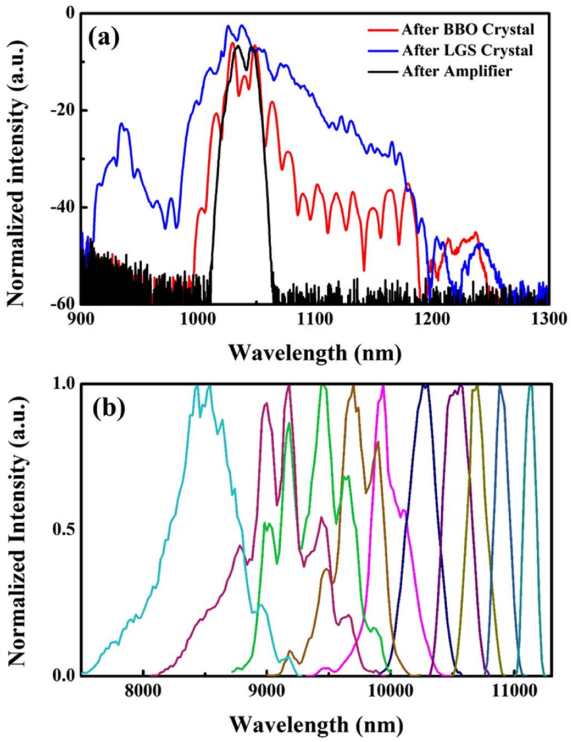

Fig. 6. (a) Measured spectra of driving pulses plotted in logarithmic scale from the regenerative amplifier (black), after the BBO cascaded-quadratic compressor (red), and after the 8 mm thick LGS crystal (blue). (b) The measured MIR spectra with different phase-matching angles tuning in the wavelength range of 7.5–11.2 μm.

phase-matching bandwidth pumped at ~1 μm wavelength, and more importantly, large bandgap energy (3.7 eV) to eliminate the strong two-photon absorption. The 50 fs driving laser is divided into two orthogonally polarized pulses on the e and o axes by an HWP, serving as the pump and signal pulses, respectively. The length of the LGS crystal is chosen as 8 mm to allow sufficient self-phase modulation and spectral broadening of both the pump and signal pulses. The near-infrared spectrum after the LGS crystal (blue curve) is measured as shown in Fig. 6(a). Compared to the incident spectrum (red curve), there is substantial spectral broadening in the wavelength range of 1100–1180 nm, which has a crucial contribution as the signal components to the MIR IPDFG. It is worth mentioning that the type I phase match generates less temporal walk-off between the pump and signal [36]. In addition, the spectral broadening and dispersion also contribute beneficially to the temporal overlap between the pump and signal pulses in a long crystal [27].

As measured in Fig. 6(b), by fine-tuning the internal phase-matching angle of the LGS crystal from 51.3° to 49.1°, the MIR emission in the range of 7.5–11.2 μm is generated. The short-wavelength MIR spectrum has broader bandwidth than that of the long-wavelength side, which is attributed to the optimum phase-matching condition centered at ~8 μm. The further extensions to the short and long wavelengths are hindered by the lack of signal component beyond 1200 nm and the absorption edge of LGS, respectively. The dips at 9.1 μm,

9.3 μm, 9.56 μm, and 9.8 μm are associated with the self-phase modulation dips of the signal spectrum at 1.174 μm, 1.171 μm, 1.167 μm, and 1.163 μm, respectively, while the signal is propagating inside the LGS crystal. IPDFG conversion from 1 to 9 μm has a power efficiency of 0.03% and a quantum efficiency of 0.27%. This is a proof-of-concept demonstration that the MIR IPDFG could be driven by the relatively long pulses, which avoids using the hollow-core fiber or photonic crystal fiber compressors. It simplifies the setup significantly and could find good applications in MIR spectroscopy. The milliwatt (mW)-scale output power also suits the spectroscopic applications well.

4. CONCLUSION

In conclusion, we demonstrate a high-power Yb:CALGO regenerative amplifier system with 11 W average power, 255 μJ pulse energy, and 50 fs pulse width at 43 kHz repetition rate. The customized Yb-fiber oscillator, specially designed spectral shaper, and Yb:CALGO gain medium with broad emission bandwidth, combined with the cascaded-quadratic compressor, enable ultrashort pulse width and 3.7 GW peak power, which to some extent bridges the gap between the Yb-doped laser and Ti:sapphire laser. It is suggested that there is still large headroom for the power upscaling with the readily available high-power laser diode, large aperture and good thermal conductivity of Yb:CALGO crystal, as well as the self-defocusing nature of the cascaded-quadratic compression. Further amplification of sub-50 fs pulses with $>$ 50 W average power and $>$ 1 mJ pulse energy would be expected in the near future, which could serve as an alternative to the Ti:sapphire laser with higher average power. In addition, with a long LGS crystal providing sufficient seed spectral broadening, and a phase-matching condition with smaller temporal walk-off, a proof-of-concept demonstration of MIR IPDFG tuning in the range of 7.5–11.2 μm is performed driven by the 50 fs laser. Without the necessity of the sophisticated fiber compressors, the MIR IPDFG is significantly simplified, and more MIR spectroscopic applications could be pursued based on the demonstrated technique.

Funding. National Natural Science Foundation of China (62075144); Engineering Featured Team Fund of Sichuan University (2020SCUNG105).

Disclosures. The authors declare no conflicts of interest.

REFERENCES

1. K. Liu, H. Li, S. Z. Qu, H. K. Liang, Q. J. Wang, and Y. Zhang, "20 W, 2 mJ, sub-ps, 258 nm all-solid-state deep-ultraviolet laser with up to 3 GW peak power," Opt. Express **28**, 18360–18367 (2020).
2. I. Pupeza, D. Sánchez, J. Zhang, N. Lilienfein, M. Seidel, N. Karpowicz, T. Paasch-Colberg, I. Znakovskaya, M. Pescher, W. Schweinberger, V. Pervak, E. Fill, O. Pronin, Z. Wei, F. Krausz, A. Apolonski, and J. Biegert, "High-power sub-two-cycle mid-infrared pulses at 100 MHz repetition rate," Nat. Photonics **9**, 721–724 (2015).
3. M. Seidel, X. Xiao, S. A. Hussain, G. Arisholm, A. Hartung, K. T. Zawilski, P. G. Schunemann, F. Habel, M. Trubetskov, V. Pervak, O. Pronin, and F. Krausz, "Multi-watt, multi-octave, mid-infrared femtosecond source," Sci. Adv. **4**, eaaq1526 (2018).
4. B. Zhang, Z. Ma, J. Ma, X. Wu, C. Ouyang, D. Kong, T. Hong, X. Wang, P. Yang, L. Chen, Y. Li, and J. Zhang, "1.4 mJ high energy terahertz radiation from lithium niobates," Laser Photon. Rev. **15**, 2000295 (2021).
5. T. Popmintchev, M. Chen, D. Popmintchev, P. Arpin, S. Brown, S. Ališauskas, G. Andriukaitis, T. Balčiunas, O. D. Mücke, A. Pugzlys, A. Baltuška, B. Shim, S. E. Schrauth, A. Gaeta, C. H. García, L. Plaja, A. Becker, A. J. Becker, M. M. Murnane, and H. C. Kapteyn, "Bright coherent ultrahigh harmonics in the keV X-ray regime from mid-infrared femtosecond lasers," Science **336**, 1287–1291 (2012).
6. T. Gaumnitz, A. Jain, Y. Pertot, M. Huppert, I. Jordan, F. Ardana-Lamas, and H. J. Wörner, "Streaking of 43-attosecond soft-X-ray pulses generated by a passively CEP-stable mid-infrared driver," Opt. Express **25**, 27506–27518 (2017).
7. M. Cho, "Coherent two-dimensional optical spectroscopy," Chem. Rev. **108**, 1331–1418 (2008).
8. V. Cardinali, E. Marmois, B. Le Garrec, and G. Bourdet, "Determination of the thermo-optic coefficient dn/dT of ytterbium doped ceramics (Sc_2O_3, Y_2O_3, Lu_2O_3, YAG), crystals (YAG, CaF_2) and neodymium doped phosphate glass at cryogenic temperature," Opt. Mater. **34**, 990–994 (2012).
9. S. Cho, J. Jeong, S. Hwang, and T. J. Yu, "Thermal lens effect model of Ti:sapphire for use in high-power laser amplifiers related content," Appl. Phys. Express **11**, 092701 (2018).
10. T. Nubbemeyer, M. Kaumanns, M. Ueffing, M. Gorjan, A. Alismail, H. Fattahi, J. Brons, O. Pronin, H. G. Barros, Z. Major, T. Metzger, D. Sutter, and F. Krausz, "1 kW, 200 mJ picosecond thin-disk laser system," Opt. Lett. **42**, 1381–1384 (2017).
11. Y. Wang, H. Chi, C. Baumgarten, K. Dehne, A. R. Meadows, A. Davenport, G. Murray, B. A. Reagan, C. S. Menoni, and J. J. Rocca, "1.1 J Yb:YAG picosecond laser at 1 kHz repetition rate," Opt. Lett. **45**, 6615–6618 (2020).
12. B. Schmidt, A. Hage, T. Mans, F. Légaré, and H. Wörner, "Highly stable, 54 mJ Yb-InnoSlab laser platform at 0.5 kW average power," Opt. Express **25**, 17549–17555 (2017).
13. E. Kaksis, G. Almási, J. A. Fülöp, A. Pugžlys, A. Baltuška, and G. Andriukaitis, "110-mJ 225-fs cryogenically cooled Yb:CaF_2 multipass amplifier," Opt. Express **24**, 28915–28922 (2016).
14. M. Siebold, S. Bock, U. Schramm, B. Xu, J. L. Doualan, P. Camy, and R. Moncorgé, "Yb:CaF_2 — a new old laser crystal," Appl. Phys. B **97**, 327–338 (2009).
15. G. H. Kim, J. Yang, S. A. Chizov, A. V. Kulik, E. G. Sall, V. E. Yashin, and U. Kang, "High peak and high average power Yb:KGW laser systems for industrial applications," in *International Conference Laser Optics* (2014), p. 1.
16. H. He, J. Yu, W. Zhu, X. Guo, C. Zhou, and S. Ruan, "A Yb:KGW dual-crystal regenerative amplifier," High Power Laser Sci. Eng. **8**, e35 (2020).
17. R. Akbari and A. Major, "High-power diode-pumped Kerr-lens mode-locked bulk Yb:KGW laser," Appl. Opt. **56**, 8838–8844 (2017).
18. A. Greborio, A. Guandalini, and J. Aus der Au, "Sub-100 fs pulses with 12.5 W from Yb:CALGO based oscillators," Proc. SPIE **8235**, 823511 (2012).
19. S. Manjooran and A. Major, "Diode-pumped 45 fs Yb:CALGO laser oscillator with 1.7 MW of peak power," Opt. Lett. **43**, 2324–2327 (2018).
20. E. Caracciolo, A. Guandalini, F. Pirzio, M. Kemnitzer, F. Kienle, A. Agnesi, and J. Aus der Au, "High power Yb:CALGO ultrafast regenerative amplifier for industrial application," Proc. SPIE **10082**, 100821F (2017).
21. W. Tian, R. Xu, L. Zheng, X. Tian, D. Zhang, X. Xu, J. Zhu, J. Xu, and Z. Wei, "10-W-scale Kerr-lens mode-locked Yb:CALYO laser with sub-100-fs pulses," Opt. Lett. **46**, 1297–1300 (2021).
22. A. Rudenkov, V. Kisel, A. Yasukevich, K. Hovhannesyan, A. Petrosyan, and N. Kuleshov, "Yb:CALYO-based femtosecond chirped pulse regenerative amplifier for temporally resolved pump-probe spectroscopy," Devices Methods Meas. **9**, 205–214 (2018).
23. E. Caracciolo, F. Pirzio, M. Kemnitzer, M. Gorjan, A. Guandalini, F. Kienle, A. Agnesi, and J. Aus Der Au, "42 W femtosecond Yb:Lu_2O_3 regenerative amplifier," Opt. Lett. **41**, 3395–3398 (2016).
24. I. J. Graumann, A. Diebold, C. G. E. Alfieri, F. Emaury, B. Deppe, M. Golling, D. Bauer, D. Sutter, C. Kränkel, C. J. Saraceno, C. R. Phillips,

and U. Keller, "Peak-power scaling of femtosecond Yb:Lu_2O_3 thin-disk lasers," Opt. Express **25**, 22519–22536 (2017).
25. P. Loiko, F. Druon, P. Georges, B. Viana, and K. Yumashev, "Thermo-optic characterization of Yb:$CaGdAlO_4$ laser crystal," Opt. Mater. Express **4**, 2241–2249 (2014).
26. J. Pouysegur, M. Delaigue, Y. Zaouter, C. Hönninger, E. Mottay, A. Jaffrès, P. Loiseau, B. Viana, P. Georges, and F. Druon, "Sub-100-fs Yb:CALGO nonlinear regenerative amplifier," Opt. Lett. **38**, 5180–5183 (2013).
27. B. H. Chen, T. Nagy, and P. Baum, "Efficient middle-infrared generation in $LiGaS_2$ by simultaneous spectral broadening and difference-frequency generation," Opt. Lett. **43**, 1742–1745 (2018).
28. C. Gaida, M. Gebhardt, T. Heuermann, F. Stutzki, C. Jauregui, J. Antonio-Lopez, A. Schülzgen, R. Amezcua-Correa, A. Tünnermann, I. Pupeza, and J. Limpert, "Watt-scale super-octave mid-infrared intrapulse difference frequency generation," Light Sci. Appl. **7**, 94 (2018).
29. J. Zhang, K. F. Mak, N. Nagl, M. Seidel, D. Bauer, D. Sutter, V. Pervak, F. Krausz, and O. Pronin, "Multi-mW, few-cycle mid-infrared continuum spanning from 500 to 2250 cm^{-1}," Light Sci. Appl. **7**, 17180 (2018).
30. S. Vasilyev, I. S. Moskalev, V. O. Smolski, J. M. Peppers, M. Mirov, A. V. Muraviev, P. G. Schunemann, S. B. Mirov, K. L. Vodopyanov, and V. P. Gapontsev, "Super-octave longwave mid-infrared coherent transients produced by optical rectification of few-cycle 2.5-μm pulses," Optica **6**, 111–114 (2019).
31. Y. G. Jeong, R. Piccoli, D. Ferachou, V. Cardin, M. Chini, S. Hädrich, J. Limpert, R. Morandotti, F. Légaré, B. E. Schmidt, and L. Razzari, "Direct compression of 170-fs 50-cycle pulses down to 1.5 cycles with 70% transmission," Sci. Rep. **8**, 11794 (2018).
32. S. Gröbmeyer, K. Fritsch, B. Schneider, M. Poetzlberger, V. Pervak, J. Brons, and O. Pronin, "Self-compression at 1 μm wavelength in all-bulk multi-pass geometry," Appl. Phys. B **126**, 159 (2020).
33. F. W. Wise and J. Moses, "Self-focusing and self-defocusing of femtosecond pulses with cascaded quadratic nonlinearities," in *Self-focusing: Past and Present* (Springer, 2009), Vol. **114**, pp. 481–506.
34. X. Liu, L. Qian, and F. W. Wise, "High-energy pulse compression by use of negative phase shifts produced by the cascaded $\chi^{(2)}:\chi^{(2)}$ nonlinearity," Opt. Lett. **24**, 1777–1779 (1999).
35. P. Raybaut, F. Balembois, F. Druon, and P. Georges, "Numerical and experimental study of gain narrowing in ytterbium-based regenerative amplifiers," IEEE J. Quantum Electron. **41**, 415–425 (2005).
36. K. Kato, K. Miyata, L. I. Isaenko, S. Lobanov, V. N. Vedenyapin, and V. Petrov, "Phase-matching properties of $LiGaS_2$ in the 1.025–10.5910 μm spectral range," Opt. Lett. **42**, 4363–4366 (2017).